ESR Dating of Barite in Sea-Floor Hydrothermal Sulfide Deposits in the Okinawa Trough

29

Taisei Fujiwara, Shin Toyoda, Ai Uchida, Jun-ichiro Ishibashi, Shun'ichi Nakai, and Asako Takamasa

Abstract

ESR (electron spin resonance) ages were determined for barite crystals extracted from hydrothermal sulfide deposits taken at Daiyon-Yonaguni Knoll field, Hatoma Knoll field, Iheya North Knoll field, Hakurei Site of Izena Hole field, Yoron Hole field of the Okinawa Trough. The ages range from 4.1 to 16,000 years, being consistent with detection of ^{228}Ra in younger samples and radioactive equilibrium/disequilibrium between radium and daughter nuclei. The variation of the ages within each sample is mostly within the statistical error range. The relative order of the ages is consistent with the result of ^{226}Ra-^{210}Pb method, but the determining absolute ages is still an issue. The order of ages of the 5 hydrothermal fields would be arranged, from young to old as follows; Yoron Hole field, Daiyon-Yonaguni Knoll field, Hatoma Knoll field, being nearly equal to Iheya North Knoll field.

Keywords

Barite • Dating • Electron spin resonance • Hydrothermal activities

29.1 Introduction

There have been many scientific efforts devoted for studies on active sea-floor hydrothermal fields found in Okinawa Trough (Ishibashi et al. Chap. 23). The evolution of these hydrothermal fields is one of the important issues. Dating methods have been employed for hydrothermal sulfide deposits, such as the U-Th disequilibrium method (e.g. You and Bickle 1998) applicable for the age range more than several thousand years, and ^{226}Ra-^{210}Pb and ^{228}Ra-^{228}Th method (e.g. Noguchi et al. 2011) for the range less than 150 years. The age range of several hundred years is essential to estimate the life time of hydrothermal activities. However, dating methods for the age range are lacking.

Okumura et al. (2010) made the first practical application of ESR dating technique to a sample of seafloor hydrothermal barite to obtain ages of 300 and 3,620 years, while Kasuya et al. (1991) first pointed out that barite can be used for ESR dating. Toyoda et al. (2011) determined the optimum ESR condition while Sato et al. (2011) confirmed that the signal is thermally stable enough for an age range of several thousand years.

Seafloor massive sulfide deposits are composed of sulfide minerals such as pyrite, sphalerite, chalcopyrite and galena, and also include sulfate minerals such as anhydrite and barite. The sulfate minerals precipitate by mixing of hydrothermal fluid and seawater, while the sulfide minerals precipitate from the hydrothermal fluid mainly by cooling (Hannington et al. 1995). It is generally considered that a combination and/or switch of these two modes of hydrothermal precipitation lead to growth of sulfide structures such as a chimney and mound and that of large hydrothermal

T. Fujiwara • S. Toyoda (✉) • A. Uchida
Okayama University of Science, Okayama, Japan
e-mail: toyoda@dap.ous.ac.jp

J.-i. Ishibashi
Kyusyu University, Fukuoka, Japan

S. Nakai
University of Tokyo, Tokyo, Japan

A. Takamasa
National Institute of Radiological Sciences, Chiba, Japan

J.-i. Ishibashi et al. (eds.), *Subseafloor Biosphere Linked to Hydrothermal Systems: TAIGA Concept*,
DOI 10.1007/978-4-431-54865-2_29,

deposits (e.g. Tivey 2007). Takamasa et al. (2013) determined ESR ages for barite in sulfide deposits in the South Mariana Trough hydrothermal field, and concluded that the ages are consistent with U-Th ages. In this study, the ages of various hydrothermal sulfides in the Okinawa Trough are determined by ESR dating.

29.2 Material and Methods

The sulfide deposit samples were obtained in the 6 research cruises; NT01-05, NT02-07, YK04-05, NT11-20, NT12-06, and NT12-10 operated by the Japan Agency for Marine-Earth Science and Technology (JAMSTEC) from Daiyon-Yonaguni Knoll field, Hatoma Knoll field, Iheya North Knoll field, Hakurei field of Izena Hole field, Yoron Hole field of the Okinawa Trough (Figs. 29.1 and 29.2, and Table 29.1). After blocks of sulfide sample were cut into pieces (Fig. 29.3), approximately 2.0 g of the pieces was crushed. The samples were soaked in 12 M hydrochloric acid for approximately 24 h. Then, 13 M nitric acid was added. Finally, after rinsing in distilled water, the sample was filtered and dried. Mineral grains other than barite were removed by handpicking. The purified mineral grains were determined by an X-ray diffraction and confirmed that the grains are pure barite.

The barite grains extracted from each sample were separated into 100–250 μm aliquots for gamma ray irradiation up to about 10 kGy with a dose rate of 404.4 Gy/h made at Takasaki Advanced Radiation Research Institute, Japan Atomic Energy Agency (JAEA). The sample aliquots were measured at room temperature with an ESR spectrometer (JES-PX2300) with a microwave power of 1 mW, and the magnetic field modulation amplitude of 0.1 mT as indicated by Toyoda et al. (2011) to be the best measurement conditions. The equivalent natural radiation doses were obtained by extrapolating the obtained dose response curve of the SO_3^- signal to the ordinate intercept.

The bulk radium (^{226}Ra and ^{228}Ra) concentrations were measured by the low background pure Ge gamma ray spectrometer. Assuming that Ra is populated only in barite as confirmed by Okumura et al. (2010), the internal and external dose rates of alpha, beta and gamma rays given to the barite minerals were calculated (Toyoda et al. 2014). The alpha effectiveness of 0.043 was adopted (Toyoda et al. 2012). Corrections were made for water content, beta ray attenuation for grain sizes (a plane with 20 μm in thickness as confirmed by thin section). In the present paper, a new formula is proposed to obtain the ages which takes into account the decays of ^{226}Ra (a half life of 1,600 years) and ^{228}Ra (a half life of 5.75 years) with disequilibrated daughter nuclei as the following.

29.3 The Dose Rate Conversion Factors and the Decay Corrections for ^{226}Ra and ^{228}Ra

It is the most important feature of hydrothermal barite in the aspect of dose rate estimation that the only source of the radiation is internal radium (Okumura et al. 2010; Toyoda et al. 2014). The dose rate was calculated from the concentrations of radium and its daughter nuclei as the following.

The newest dose rate conversion factors, which are to be multiplied to the concentrations of U, Th, K to obtain dose rate, were reported by Guérin et al. (2011) for U and Th in radioactive equilibrium and for K together with the contributions of each nucleus in the decay chains. Toyoda et al. (2014) obtained the dose rate conversion factors from their table for ^{226}Ra only in the case of radioactive equilibrium. By summing up the energy contributions of the nuclei in the chains listed in Guérin et al. (2011), the dose rate conversion factors for ^{226}Ra and ^{228}Ra were calculated so that the dose rate can be obtained in the case of radioactive disequilibrium as shown in Table 29.2.

When the dose rate varies with time in the past, the equivalent dose, D_E, obtained by the ESR measurements is expressed by the integration of a time dependent dose rate, D (t), as the following,

$$D_E = \int_0^T D(t)dt \tag{29.1}$$

As the source of the dose is Ra which decays with time, the decay has to be taken into account for the does rate, D(t). For the decay of ^{226}Ra, Toyoda et al. (2014) obtained a formula as

$$T = \frac{1}{\lambda}\ln\left(\lambda\frac{D_E}{D} + 1\right) \tag{29.2}$$

This formula is valid for the samples with ages over 200 years where the daughter nucleus with second longest half life (^{210}Pb, 22.3 years) in the decay series is equilibrated. However, for the younger samples, the radioactive disequilibrium and contributions from the decay series starting from ^{228}Ra have to be considered.

When the number of nuclei of ^{226}Ra or ^{228}Ra is N_1, and that of the daughter nuclei with second longest life (^{210}Pb or ^{228}Th) is N_2, those are expressed as,

$$N_1 = N_{10}\,e^{-\lambda_1 t} \tag{29.3}$$

$$N_2 = \frac{\lambda_1}{\lambda_2 - \lambda_1}N_{10}\left(e^{-\lambda_1 t} - e^{-\lambda_2 t}\right) \tag{29.4}$$

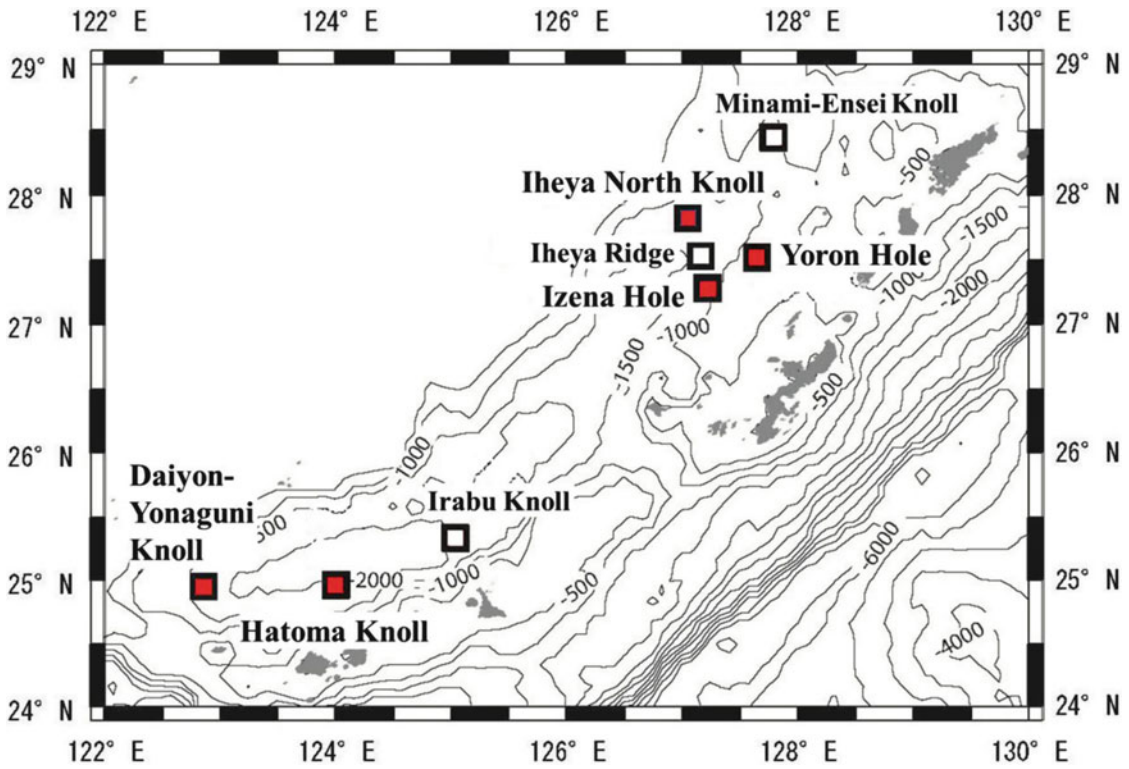

Fig. 29.1 A bathymetric map of the known hydrothermal fields and sampling fields in the Okinawa Trough. *Red triangles* indicate the sampling fields; Daiyon-Yonaguni Knoll field, Hatoma Knoll field, Iheya North Knoll field, Hakurei field of Izena Hole field, Yoron Hole field

where N_{10} is the initial number of parent nuclei, λ_1 and λ_2 are the decay constant of the parent and the daughter nuclei, respectively, and it is assumed that initially no daughter nuclei are present. We only know the number of nuclei at present, N_{1p}, expressed as,

$$N_{1p} = N_{10}e^{-\lambda_1 T}$$

where T is the age of the sample. Therefore, Eqs. (29.3) and (29.4) are written as,

$$N_1 = N_{1p}e^{\lambda_1(T-t)} \tag{29.5}$$

$$N_2 = \frac{\lambda_1}{\lambda_2 - \lambda_1}N_{1p}e^{\lambda_1 T}\left(e^{-\lambda_1 t} - e^{-\lambda_2 t}\right) \tag{29.6}$$

respectively.

The dose rate, D(t), given by the parent and daughter nuclei is written as,

$$D(t) = Q_1\lambda_1 N_1(t) + Q_2\lambda_2 N_2(t) \tag{29.7}$$

where Q_1 and Q_2 are the dose rate conversion factors for the nuclei from the parent to the one just before the daughter with the second longest life time in the decay series, and for those from that daughter and after, respectively. Please note that a conversion factor is given per unit activity, λN. From Eqs. (29.5)–(29.7) is written as,

$$D(t) = \lambda_1 N_{1p}e^{\lambda_1 T}\left\{e^{-\lambda_1 t}\left(Q_1 + Q_2\frac{\lambda_2}{\lambda_2 - \lambda_1}\right) - Q_2 e^{-\lambda_2 t}\right\} \tag{29.8}$$

The D_E is given by integrating the dose rate as the following,

$$D_E = \int_0^T D(t)dt$$

$$= \lambda_1 N_{1p}e^{\lambda_1 T}\left\{\frac{1}{\lambda_1}\left(Q_1 + Q_2\frac{\lambda_2}{\lambda_2 - \lambda_1}\right)\left(1 - e^{-\lambda_1 T}\right) - \frac{Q_2}{\lambda_2}\left(1 - e^{-\lambda_2 T}\right)\right\} \tag{29.9}$$

For the present case, two decay series have to be taken into account, one starting from ^{226}Ra (half life: 1,600 years) where the daughter nucleus with the second longest life time is ^{210}Pb (22.3 years), and the other from ^{228}Ra (5.75 years) where the daughter is ^{228}Th (1.91 years). In the present work, the dose rates from both series are summed and T is obtained by Eq. (29.9) where the present radium activities ($\lambda_1 N_1$) were used.

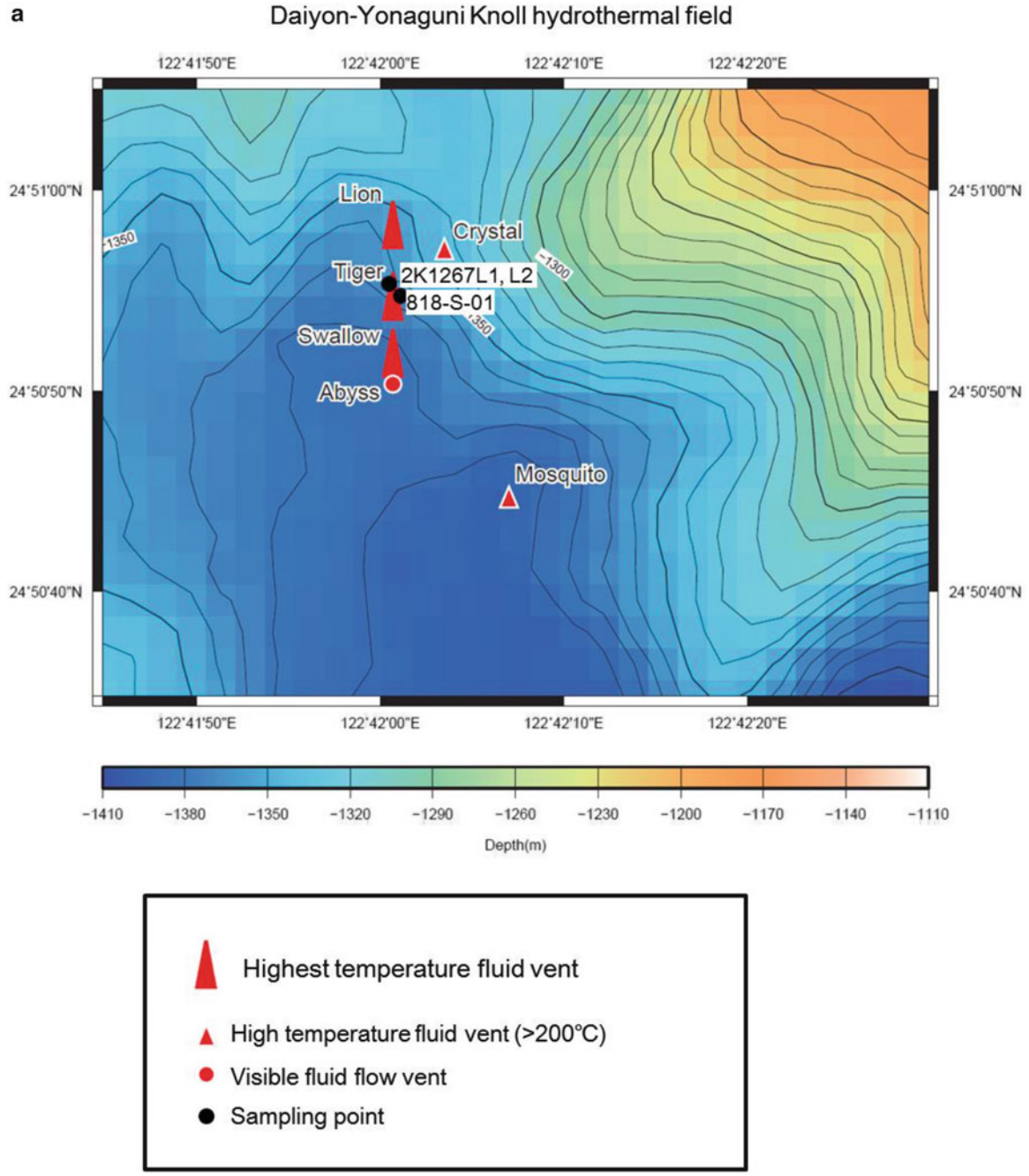

Fig. 29.2 Sampling location at the five hydrothermal fields in the Okinawa Trough. (**a**) Daiyon-Yonaguni Knoll field, (**b**) Hatoma Knoll field, (**c**) Iheya North Knoll field, (**d**) Hakurei field of Izena Hole field, (**e**) Yoron Hole field

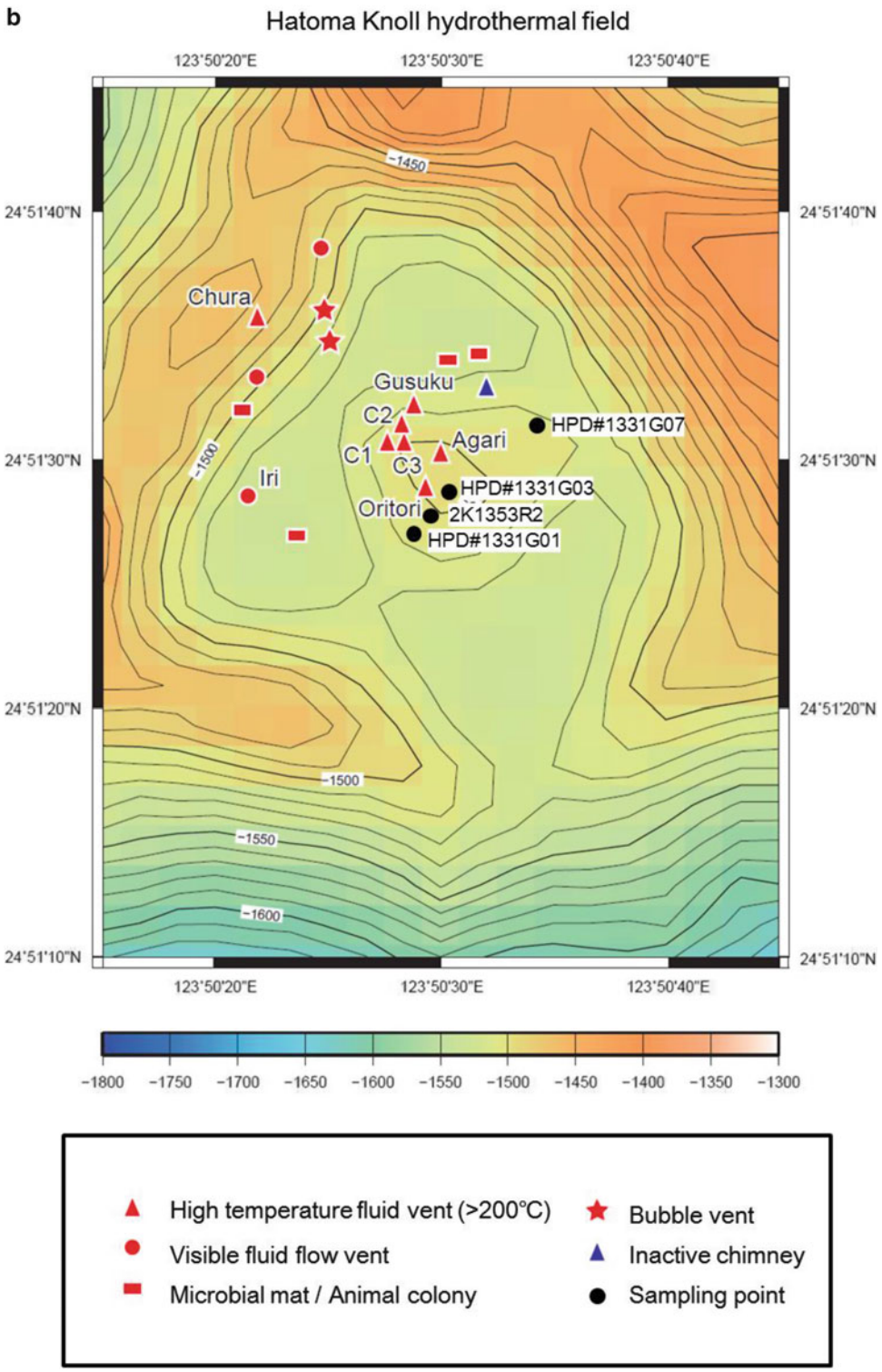

Fig. 29.2 (continued)

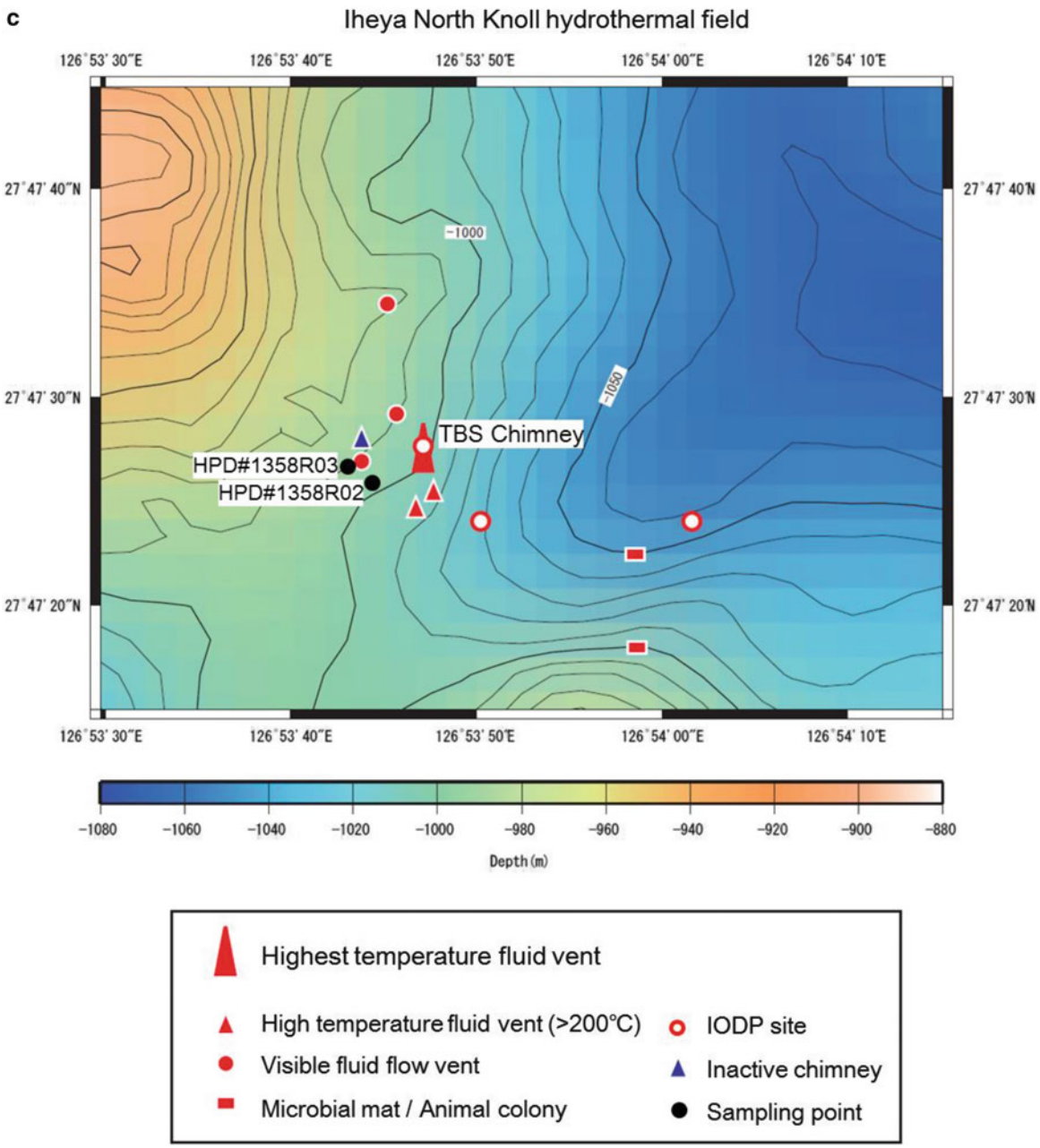

Fig. 29.2 (continued)

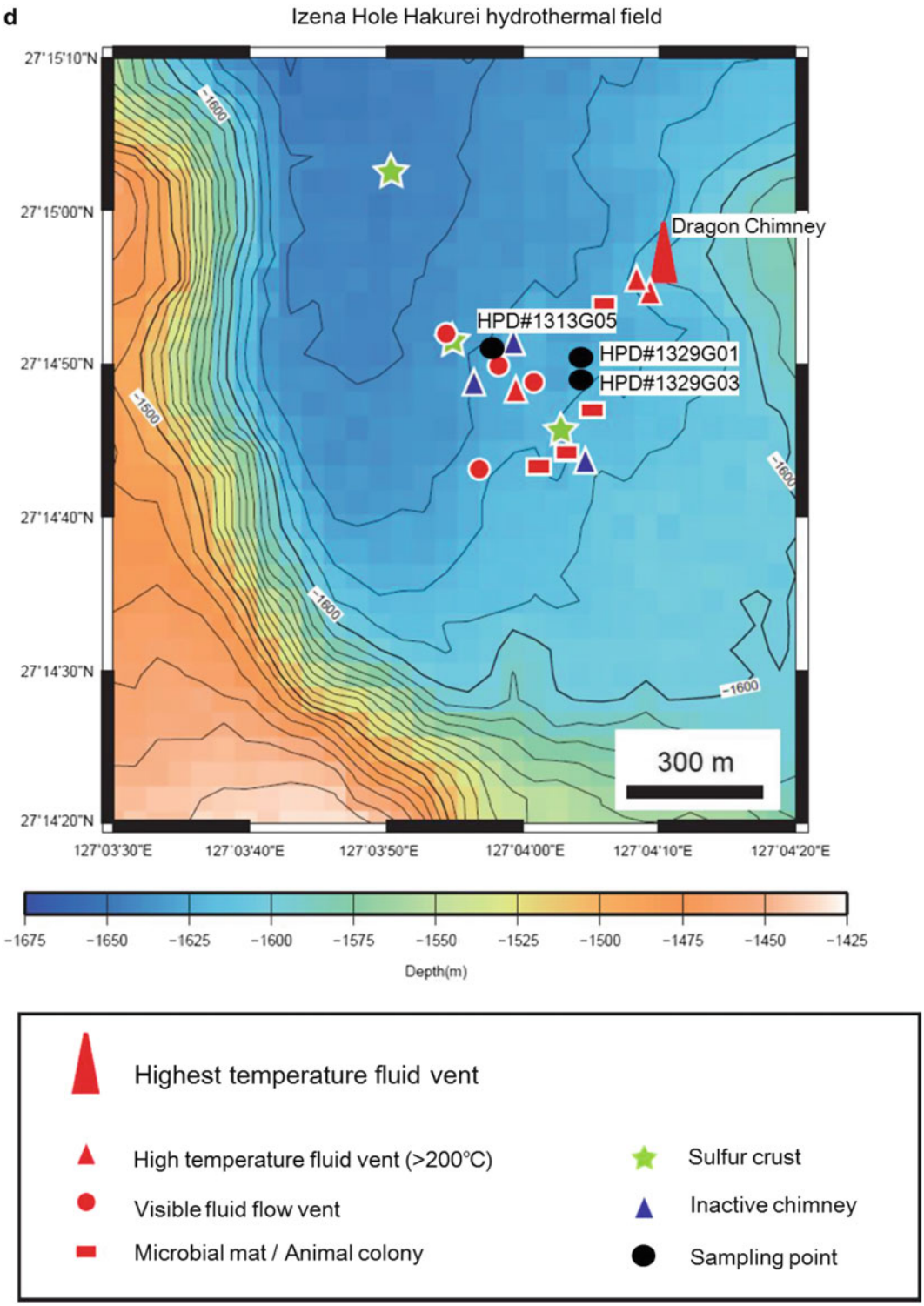

Fig. 29.2 (continued)

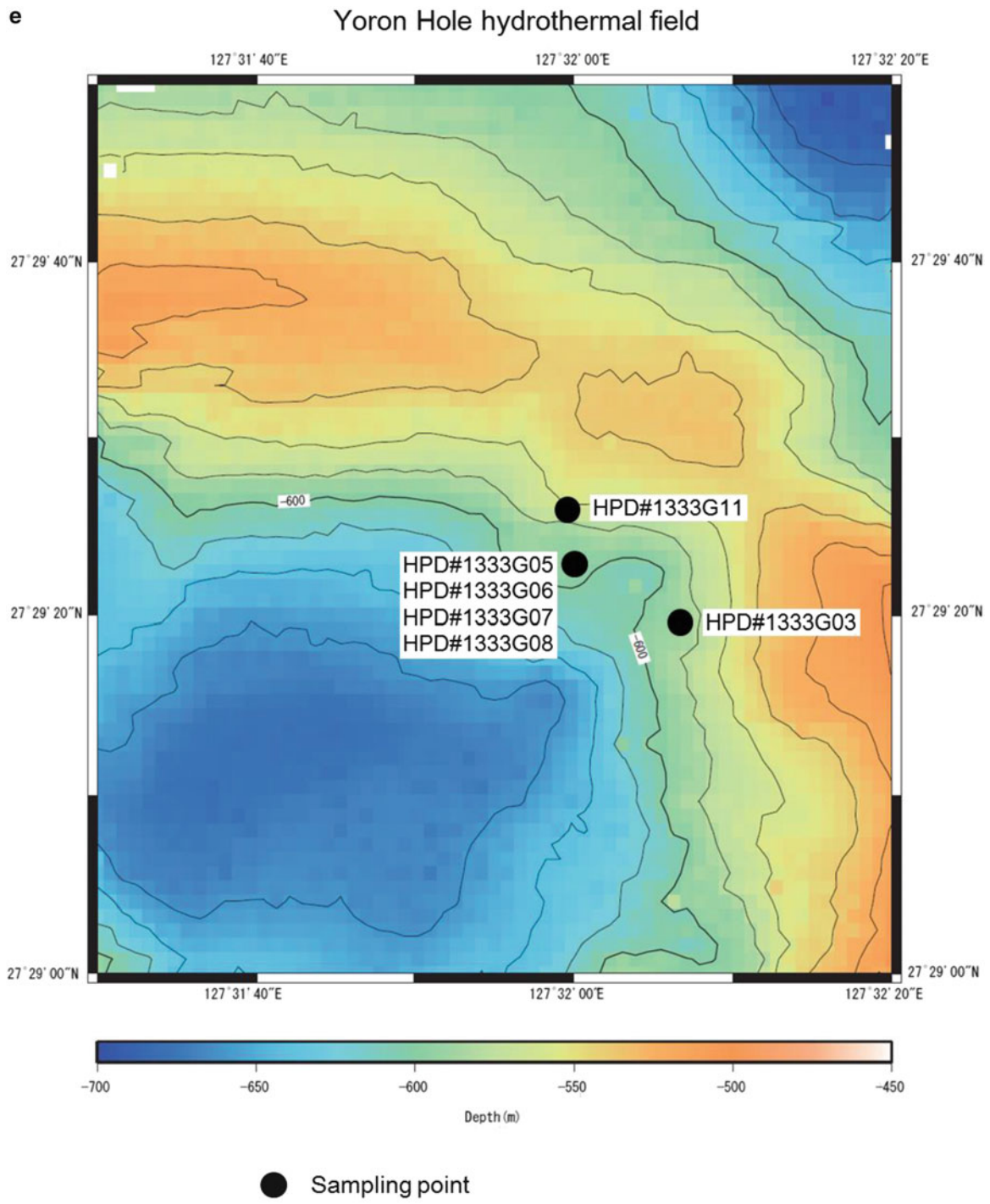

Fig. 29.2 (continued)

Table 29.1 List of samples analyzed in the present study

Sample No.	Sampling position		Depth (m)	Sampling	Sampling	Description
	Latitude (N)	Longitude (E)		Date	Tool	
Yonaguni Knoll field-Daiyon						
818-S-01	24°50.893′	122°42.020′	1,363	5/28/2004	SHINKAI6500	Active chimney
2K1267L1	24°50.934′	122°42.012′	1,366	5/16/2001	SHINKAI2000	Active chimney
2K1267L2	24°50.934′	122°42.012′	1,366	5/16/2001	SHINKAI2000	Active chimney
Hatoma Knoll field						
HPD#1331G01	24°51.450′	123°50.478′	1,499	10/8/2011	Hyper Dolphyn	Inactive chimney
HPD#1331G03	24°51.477′	123°50.508′	1,477	10/8/2011	Hyper Dolphyn	Sulfide mound
HPD#1331G07	24°51.520′	123°50.559′	1,490	10/8/2011	Hyper Dolphyn	Active chimney
2K1353R2	24°51.455′	123°50.477′	1,488	5/28/2002	SHINKAI2000	Active chimney
Iheya North Knoll field						
HD#1358R2	27°47.438′	126°53.736′	990	3/21/2012	Hyper Dolphyn	Sulfide mound
HD#1358R3	27°47.460′	126°53.730′	982	3/21/2012	Hyper Dolphyn	Inactive chimney
Izena Hole field						
HPD#1313G05	27°14.856′	127°03.962′	1,613	8/22/2011	Hyper Dolphyn	Active chimney
HPD#1329G01	27°14.838′	127°04.093′	1,620	10/5/2011	Hyper Dolphyn	Inactive chimney
HPD#1329G03	27°14.815′	127°03.093′	1,617	10/5/2011	Hyper Dolphyn	Inactive chimney
Yoron Hole field						
HPD#1333G03	27°29.328′	127°32.124′	580	10/10/2011	Hyper Dolphyn	Active chimney
HPD#1333G05	27°29.382′	127°32.004′	591	10/10/2011	Hyper Dolphyn	Active chimney
HPD#1333G06	27°29.382′	127°32.004′	591	10/10/2011	Hyper Dolphyn	Active chimney
HPD#1333G07	27°29.382′	127°32.004′	591	10/10/2011	Hyper Dolphyn	Active chimney
HPD#1333G08	27°29.382′	127°32.004′	591	10/10/2011	Hyper Dolphyn	Active chimney
HPD#1333G11	27°29.424′	127°31.998′	566	10/10/2011	Hyper Dolphyn	Active chimney

29.4 Results and Discussions

A typical ESR spectrum is shown in Fig. 29.4. The principal g factors are calculated from this powder spectrum to be 1.9995, 2.0023, and 2.0031, being consistent with the g factors for SO_3^- radical obtained by Krystec (1980), which are 1.9995, 2.0023, and 2.0032. The peak-to-peak height of the spectrum (Fig. 29.4) was used as the signal intensity. An example of dose response of the signal intensity is shown in Fig. 29.5. Extrapolating the dose response to the zero ordinate, being fitted by a saturating exponential curve, the equivalent doses are obtained as shown in Table 29.3.

The ^{226}Ra and ^{228}Ra concentrations were measured by a low background pure germanium gamma ray spectrometer for bulk samples as shown in Table 29.3. The ^{226}Ra concentrations were obtained from the peak counts for ^{214}Bi (609, 1,120, 1,765 keV) and for ^{214}Pb (295 and 352 keV) in comparison with a standard uranite sample with radioactive equilibrium with known uranium concentration. The ^{228}Ra concentrations were from the peak counts for ^{228}Ac (338, 911, 969 keV) (Yonezawa et al. 2002). The ages of the samples were determined using the Eq. (29.6) as shown in Table 29.3.

The ages ranged from 4.1 to 16,000 years while the ages of pieces from a sample varies more than estimated analytical errors (Table 29.3). As discussed by Toyoda et al. (2014), microscopic observation revealed that sulfide minerals with various size and various occurrence fill the spaces among barite crystals, suggesting repeated stages of mineralization, which starts with sulfate precipitation and followed by sulfide precipitation. Thus the samples would consist of minerals in various ages. It would be more probable that the determined ages are somewhat "averaged" within the portion of the sample, implying that the variation in ages corresponds to the ratio of the younger to older crystals. Therefore, when the ages vary within a sample portion, it would mean that repeated hydrothermal activities have formed the sample at the time of around those ages. If this is the case, the oldest age would correspond to the youngest limit of the oldest activity.

The determined ESR ages are young up to 56 years for those samples in which ^{228}Ra is detected. It is consistent that younger samples contain ^{228}Ra with a short half life of 5.75

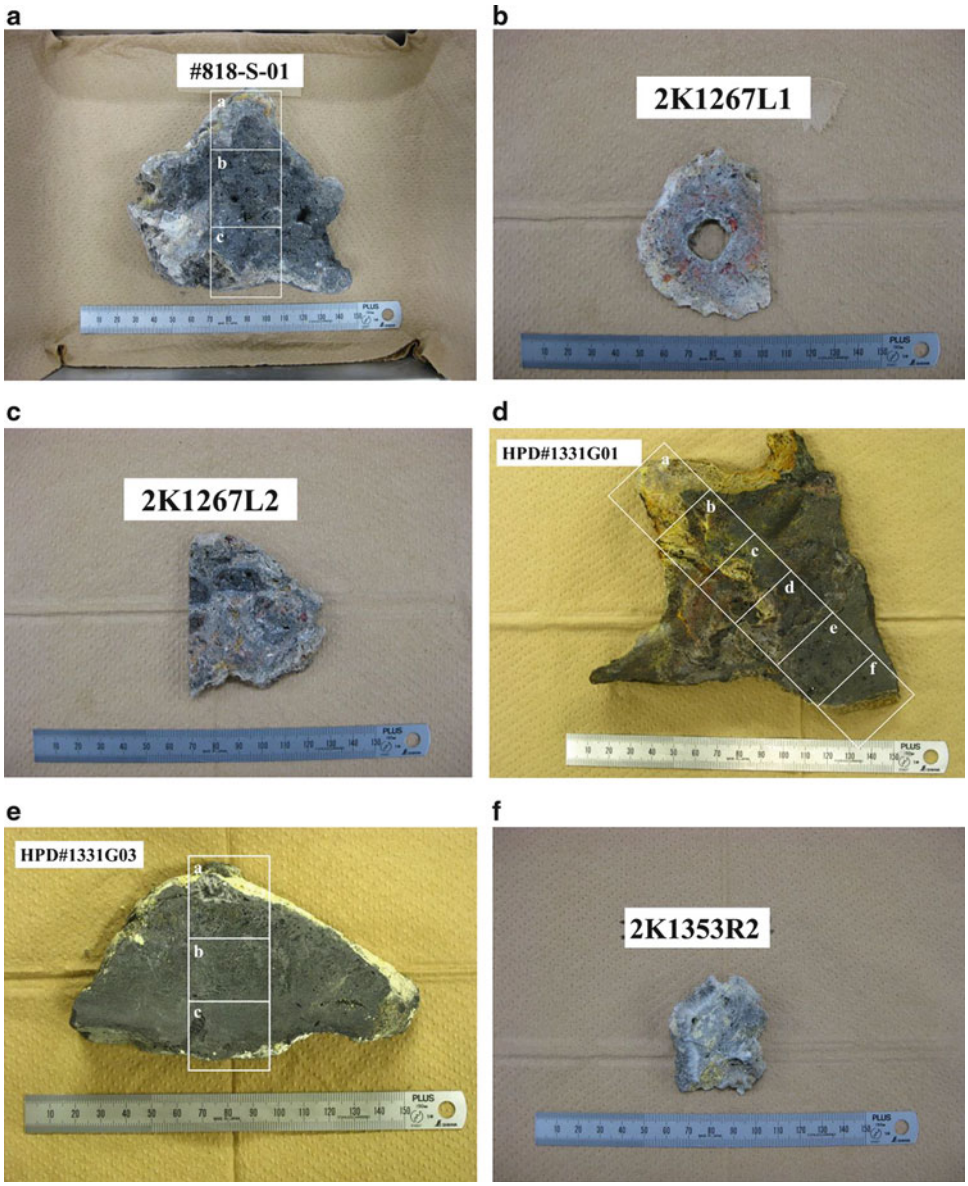

Fig. 29.3 Overview of sulfide samples and analyzed parts in each sulfide

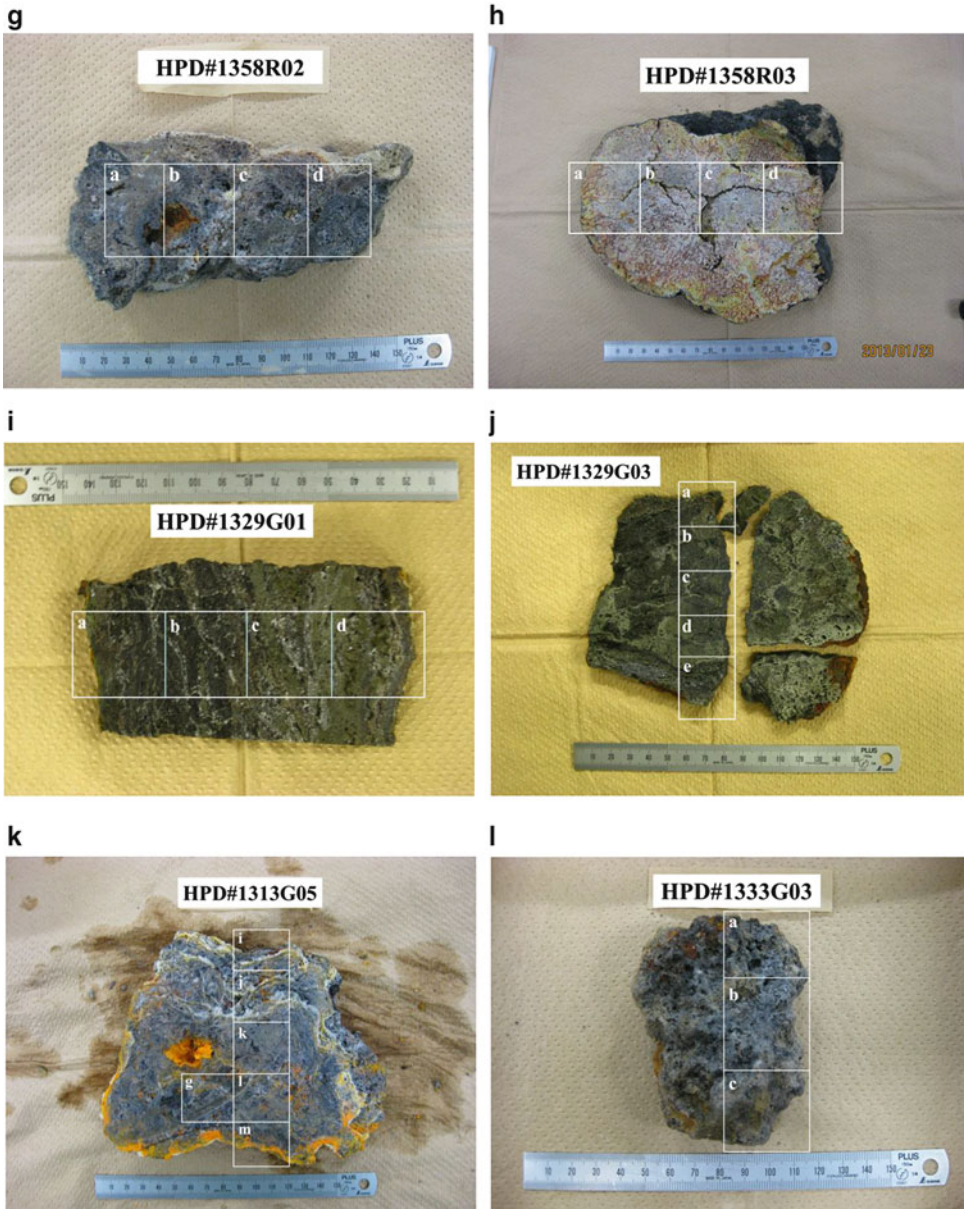

Fig. 29.3 (continued)

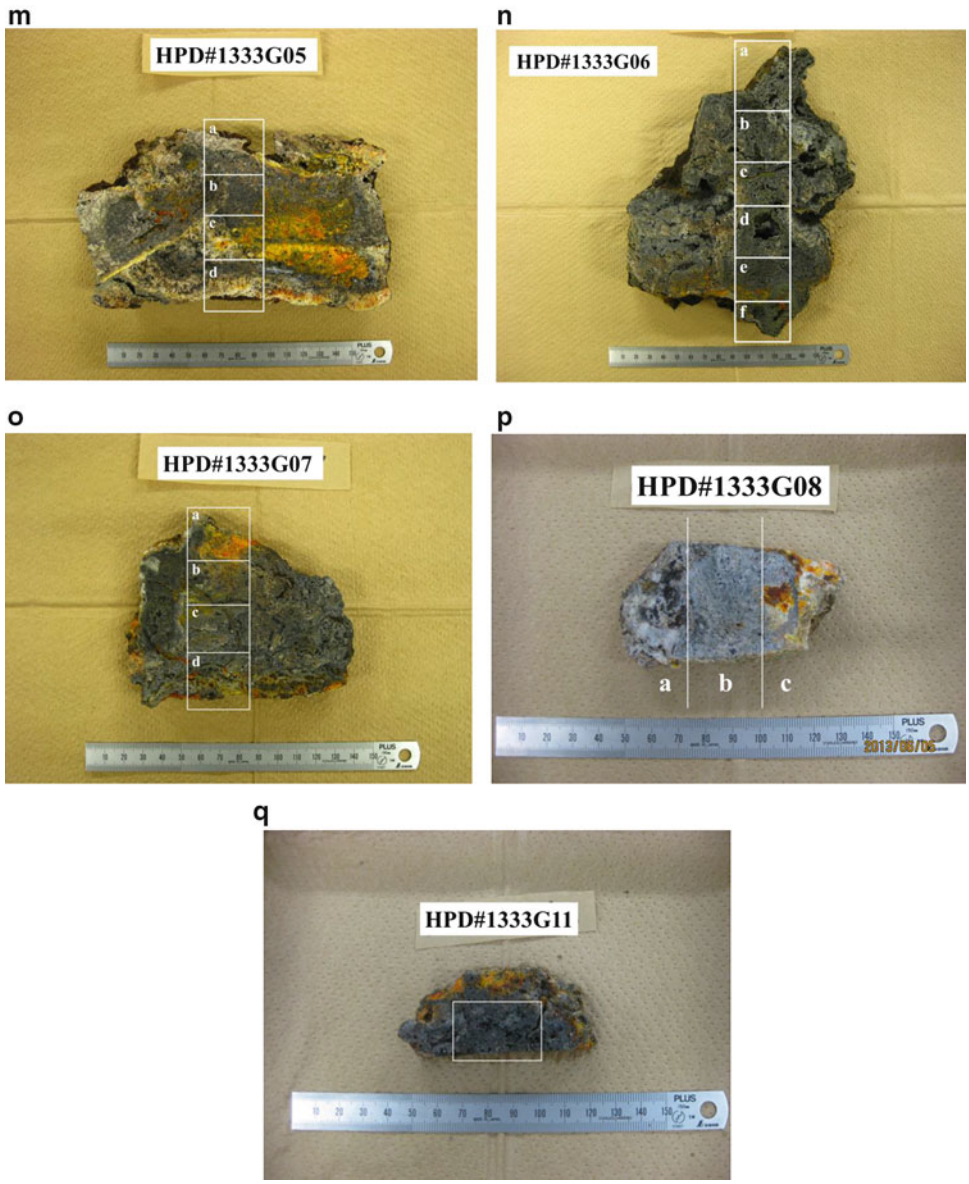

Fig. 29.3 (continued)

years. It is also reasonable that the all ESR ages for sulfide samples of active vent site are younger than those for sulfide samples of inactive vent site. ^{226}Ra-^{210}Pb and ^{228}Ra-^{228}Th ages obtained for part of the present samples are discussed in comparison with the present ESR ages by Uchida et al. (Chap. 47).

29.4.1 Daiyon-Yonaguni Knoll Field

The age of active chimney (818-S-01) from an active vent site ranges from 580 to 990 years, while the samples from active vent sites (2K1267L1, 2) show younger ages, 200 and 260 years.

29.4.2 Hatoma Knoll Field

The ESR ages of inactive chimney (HPD#1331G01) were 2,400–3,700 years, which are statistically indistinguishable. ^{210}Pb in this sample was in radioactive equilibrium with ^{226}Ra. One piece from sulfide mound sample, HPD#1331G03, shows an age of 990 years, which was statistically younger than other two ages of 3,000 and

5,700 years. The age of 2K1353R2 was determined to be 970 years. The age of HPD#1331G07 taken from an active chimney was determined to be of 7.1 years. U-Th ages were determined for sulfide minerals extracted from three pieces of HPD#1331G01, but they vary much more than ESR ages.

Table 29.2 The dose rate conversion factors in mGy/y calculated, summing up the energy contributions of the nuclei in the chains listed in Guérin et al. (2011), the dose rate conversion factors for ^{226}Ra and ^{228}Ra were calculated so that the dose rate can be obtained in the case of radiative disequilibrium

mGy/y	D_α	D_β	D_γ
^{226}Ra-^{210}Tl			
per 1 Bq/g of ^{226}Ra	120.9	4.789	8.703
per 1 ppm of virtually equilibrated ^{238}U	1.505	0.0596	0.1083
^{210}Pb-^{206}Pb			
per 1 Bq/g of ^{226}Ra	26.76	2.138	0.0241
per 1 ppm of virtually equilibrated ^{238}U	0.333	0.0266	0.0003
^{228}Ra-^{228}Ac			
per 1 Bq/g of ^{228}Ra	0	2.177	4.353
per 1 ppm of virtually equilibrated ^{232}Th	0	0.0088	0.0176
^{228}Th-^{208}Pb			
per 1 Bq/g of ^{228}Ra	162.1	4.600	7.470
per 1 ppm of virtually equilibrated ^{232}Th	0.6554	0.0186	0.0302

29.4.3 Iheya North Knoll Field

A sample from an inactive chimney (HPD#1358R3) shows ages from 3,000 to 4,300 years, while the other sample taken from a sulfide mound (HPD#1358R2) shows younger age 560–1,000 years, which are also statistically indistinguishable.

29.4.4 Izena Hole Field

Two samples from an inactive chimney (HPD#1329G01, G03) show ages over 10,000 years. On the other hand, a sample from an active chimney (HPD#1313G05) shows statistically consistent ages from 12 to 16 years, in which ^{228}Ra was also detected. ^{228}Th was equilibrated with ^{228}Ra.

29.4.5 Yoron Hole Field

The samples analyzed in the present study were all from active chimneys. Older ages over 70 years were determined for HPD#1333G05 and G06 in which no ^{228}Ra was detected while younger ages up to 56 years were determined for HPD#1333G03, G07, G08 and for HPD#1333G11 in

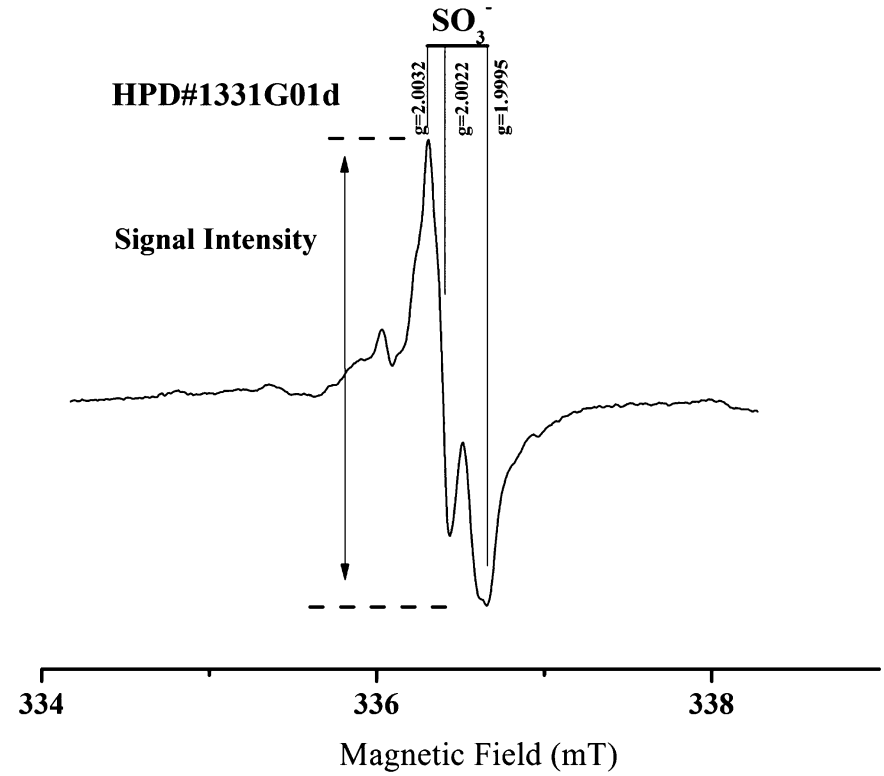

Fig. 29.4 A typical ESR spectrum in hydrothermal barite (natural sample of HPD#1331G01d)

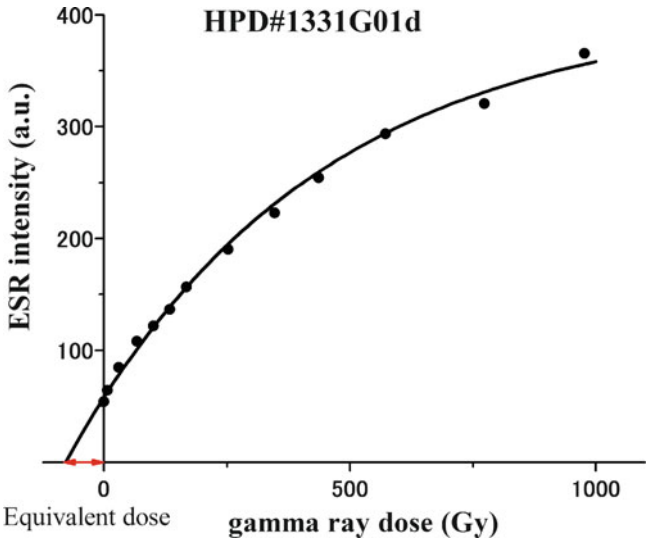

Fig. 29.5 A typical dose response of the SO_3^- signal on gamma ray dose (HPD#1331G01d)

which ^{228}Ra was detected. The two consistent ages of 400 years were determined from two pieces of the sample, HPD#1333G05, however, the age of 200 years from one piece is significantly younger than these ages. Another age of 330 years between these ages was also determined. It seems that there are two distinct ages of 70–80 and 120–150 years in HPD#1333G06, which are statistically distinct. U-Th ages for this sample were less than 20 or 80 years, younger than ESR ages. ^{226}Ra-^{210}Pb ages were determined for these two samples using the same barite samples for ESR measurements. The ages were 71–77 years for HPD#1333G05 and 23–27 years for HPD#1333G06, significantly younger than ESR ages, but the relative order is consistent. The ESR ages of 200–400 years for HPD#1333G05 are older than 70–150 years for HPD#1333G06, while ^{226}Ra-^{210}Pb ages for HPD#1333G05 are 71–77 years, older than 23–27 years for HPD#1333G06 (Uchida et al. Chap. 47).

The sample HPD#1333G03 shows consistent ESR ages of 4.1–5.2 years, while ^{228}Ra-^{228}Th ages were 4.5–5.2 years, being coincided with ESR ages. Three ESR ages of HPD#1333G07 were in agreement between 50 and 56 years while one piece shows significantly younger age of 28 years. ^{228}Th was in radioactive equilibrium with ^{228}Ra in these samples, which is consistent with the results that ESR ages are older than HPD#1333G03, in which ^{228}Ra and ^{228}Th are in disequilibrium. Two ESR ages, 35 and 39 years, of HPD#1333G08 are statistically consistent but one age of 27 years is younger, for which ^{228}Ra-^{228}Th was determined to be 4.2 years. ^{228}Th was in radioactive equilibrium with ^{228}Ra in the former two pieces, being consistent with ESR results.

29.4.6 ESR Ages of Hydrothermal Field in the Okinawa Trough

Figure 29.6 shows the determined ESR ages plotted as a geographical position of longitude of the hydrothermal fields. The order of ages of the 5 hydrothermal fields would be arranged, from young to old as follows; Yoron Hole field < Daiyon-Yonaguni Knoll field < Hatoma Knoll field ≒ Iheya North Knoll field < Izena Hole field. The samples from Hakurei site showed the high variation of ESR ages, indicating possible variation in the age of the hydrothermal fields, therefore, a conclusion based on analysis of a few samples from active sites may not be appropriate. More systematic dating works are necessary in each specific hydrothermal field in order to reconstruct the history of the hydrothermal activities.

29.4.7 ESR Dating of Hydrothermal Barite

Our attempt is the first study to determine such a large number of ESR ages using hydrothermal barite of many sulfide breccia samples. The results indicate that ESR dating of barite would be practically useful to investigate the history of sea-floor hydrothermal systems. The technique determines the ages more promptly than using isotopes, and is especially useful in the range from 100 to 10,000 years where ^{226}Ra-^{210}Pb method is not applicable. The present study showed that the method reveals relative order of the ages among the samples, however, additional efforts should be needed to establish the method for absolute age determination through further comparative dating studies. Moreover, it is also necessary to investigate the relationship and between the variation in ages and the occurrence of the minerals.

Acknowledgements The work was supported by TAIGA project, Grant-in-Aid for Scientific Research on innovative Areas (20109004) funded by the Ministry of Education, Culture, Sports, Science and Technology (MEXT), partly by MEXT-Supported Program for the Strategic Research Foundation at Private Universities (2011–2015, S1101036), and also by the Inter-University Program for the Joint Use of JAEA Facilities.

Table 29.3 Dating results of sulfide samples

Sample No.	Barite (%)	^{226}Ra (Bq/g)	^{228}Ra (Bq/g)	^{226}Ra Dose rate (mGy/y)				^{228}Ra Dose rate (mGy/y)				Equivalent dose (Gy)		Age (year)		U-Th	^{226}Ra-^{210}Pb	^{228}Ra-^{228}Th
				D_α	D_β	$D\gamma$	D_{total}	D_α	D_β	$D\gamma$	D_{total}							
Daiyon-Yonaguni Knoll																		
818-S-01																		
a	44.0	18.5	ud.	182	119	124	424	ud.	ud.	ud.	ud.	280	+40/−30	580	+75/−60	nm.	nm.	nm.
b	3.95	2.56	ud.	220	33.1	16.5	269	ud.	ud.	ud.	ud.	332	+90/−60	990	+210/−150	nm.	nm.	nm.
c	40.9	17.6	ud.	180	112	116	408	ud.	ud.	ud.	ud.	424	+60/−150	860	+100/−280	nm.	nm.	nm.
2K1267L1	58.3	36.6	ud.	340	264	278	882	ud.	ud.	ud.	ud.	231	+40/−30	200	+40/−30	nm.	nm.	nm.
2K1267L2	58.4	30.2	ud.	280	217	229	727	ud.	ud.	ud.	ud.	284	+30/−50	260	+140/−50	nm.	nm.	nm.
Hatoma Knoll																		
HPD#1331G01																		
a	85.3	0.773	ud.	5.47	5.42	5.87	16.8	ud.	ud.	ud.	ud.	157	+18/−15	3,700	+880/−750	18,600	—	—
b	82.9	0.925	ud.	6.68	6.50	7.03	20.2	ud.	ud.	ud.	ud.	153	+17/−15	3,300	+710/−600	nm.	—	—
c	84.8	0.858	ud.	6.09	6.01	6.51	18.6	ud.	ud.	ud.	ud.	103	+9.4/−8.2	2,800	+510/−450	nm.	—	—
d	82.9	0.831	ud.	6.00	5.84	6.31	18.1	ud.	ud.	ud.	ud.	79.2	+6.3/5.6	2,400	+300/−280	nm.	—	—
e	71.5	0.735	ud.	5.88	5.21	5.58	16.7	ud.	ud.	ud.	ud.	111	+10/−8.7	3,100	+550/−480	<20	—	—
f	56.6	0.977	ud.	9.28	7.05	7.42	23.8	ud.	ud.	ud.	ud.	106	+9.5/−8.3	2,500	+380/−340	111	—	—
HPD#1331G03																		
a	13.1	3.14	ud.	105	29.1	23.8	158	ud.	ud.	ud.	ud.	196	+130/−57	990	+680/−345	nm.	nm.	—
b	9.89	0.122	ud.	5.31	1.23	0.93	7.47	ud.	ud.	ud.	ud.	187	+90/−50	5,700	+2,100/−1,500	nm.	nm.	—
c	10.6	0.489	ud.	20.0	4.83	3.71	28.5	ud.	ud.	ud.	ud.	175	+75/−40	3,000	+1,400/−900	nm.	nm.	—
HPD#1331G07	60.8	13.3	14.8	266	166.0	199	630	146	70.4	98.5	315	7.33	+0.50/−0.47	7.05	+0.44/−0.42	nm.	nm.	nm.
2K1353R2	78.0	12.0	ud.	90.2	84.6	91.1	266	ud.	ud.	ud.	ud.	321	+50/−40	970	+117/−97.8	nm.	nm.	nm.
Iheya North Knoll																		
HD#1358R2																		
a	65.8	55.9	ud.	409	352	378	1,139	ud.	ud.	ud.	ud.	1,200	+440/−260	890	+250/−160	nm.	nm.	—
b	60.2	53.5	ud.	406	331	354	1,091	ud.	ud.	ud.	ud.	1,400	+650/−340	1,000	+360/−210	nm.	nm.	—
c	44.4	52.8	ud.	514	340	353	1,207	ud.	ud.	ud.	ud.	770.0	+200/−140	560	+130/−90	nm.	nm.	—
d	43.5	44.7	ud.	458	297	307	1,062	ud.	ud.	ud.	ud.	790.0	+220/−140	650	+150/−100	nm.	nm.	—
HD#1358R3																		
a	70.2	7.84	ud.	63.5	55.6	59.5	179	ud.	ud.	ud.	ud.	1,200	+500/−280	3,200	+620/−430	nm.	nm.	—
b	83.1	7.27	ud.	52.3	51.0	55.2	159	ud.	ud.	ud.	ud.	1,000	+720/−300	3,000	+970/−560	nm.	nm.	—
c	80.3	7.33	ud.	54.0	51.6	55.7	161	ud.	ud.	ud.	ud.	1,200	+990/−380	3,300	+1,100/−620	nm.	nm.	—
d	77.8	7.35	ud.	55.4	51.8	55.8	163	ud.	ud.	ud.	ud.	2,000	+1,270/−810	4,300	+1,500/−930	nm.	nm.	—

(*continued*)

Table 29.3 (continued)

Sample No.	Barite (%)	^{226}Ra (Bq/g)	^{228}Ra (Bq/g)	^{226}Ra Dose rate (mGy/y)				^{228}Ra Dose rate (mGy/y)				Equivalent dose (Gy)		Age (year)		U-Th	^{226}Ra-^{210}Pb	^{228}Ra-^{228}Th
				D_α	D_β	$D\gamma$	D_{total}	D_α	D_β	$D\gamma$	D_{total}							
Izena Hole																		
HPD#1313G05																		
g	49.0	15.4	16.9	141	99.2	104	344	169	106	159	435	20	+5.5/−3.7	14	+1.9/−1.5	nm.	nm.	9.3
i	71.4	17.1	20.9	118	107	116	342	158	128	196	482	18	+4.9/−3.3	12	+1.8/−1.4	nm.	nm.	7.6
j	70.9	16.8	18.4	119	107	116	342	143	114	176	432	27	+10/−5.8	16	+2.6/−2.0	nm.	nm.	8.3
k	54.3	13.1	13.5	115	86.3	91.2	292	130	87.1	131	348	18	+4.5/−3.1	15	+1.8/−1.4	nm.	nm.	11
l	65.0	14.7	14.6	115	97.1	104	316	124	93.8	143	361	15	+3.4/−2.4	13	+1.5/−1.3	nm.	nm.	9.2
m	61.1	16.5	13.9	135	110	117	362	124	89.8	136	350	18	+4.6/−3.1	14	+1.8/−1.5	nm.	nm.	10
HPD#1329G01																		
a	7.79	0.147	ud.	7.96	1.60	1.09	10.6	ud.	ud.	ud.	ud.	2,600	+600/−400	10,000	+460/−400	nm.	—	—
b	8.01	0.218	ud.	11.5	2.34	1.61	15.4	ud.	ud.	ud.	ud.	8,000	+5,700/−2,400	13,000	+1,200/−800	nm.	—	—
c	10.9	0.286	ud.	11.0	2.73	2.11	15.8	ud.	ud.	ud.	ud.	15,000	+26,000/−5,000	14,000	+2,300/−1,000	nm.	—	—
d	15.3	0.410	ud.	11.3	3.56	3.03	17.9	ud.	ud.	ud.	ud.	10,000	+20,000/−3,700	13,000	+2,500/−1,100	nm.	—	—
HPD#1329G03																		
a	14.0	0.175	ud.	5.23	1.55	1.29	8.07	ud.	ud.	ud.	ud.	3,900	+3,000/−1,200	12,000	+1,300/−860	nm.	—	—
b	6.29	0.099	ud.	6.64	1.18	0.733	8.55	ud.	ud.	ud.	ud.	8,000	+6,500/−2,500	14,000	+1,300/−850	nm.	—	—
c	5.49	0.103	ud.	7.87	1.30	0.757	9.92	ud.	ud.	ud.	ud.	6,000	+2,200/−1,300	13,000	+750/−580	nm.	—	—
d	4.96	0.081	ud.	6.83	1.07	0.595	8.50	ud.	ud.	ud.	ud.	6,500	+3,300/−1,600	13,000	+950/−690	nm.	—	—
e	25.0	0.242	ud.	4.08	1.89	1.79	7.76	ud.	ud.	ud.	ud.	25,000	+30,000/−14,000	16,000	+5,900/−1,800	nm.	—	—
Yoron Hole																		
HPD#1333G03																		
a	79.5	35.8	64.5	217	212	232	661	426	372	578	1,377	11.6	+0.88/−0.82	4.6	+0.29/−0.27	nm.	nm.	4.5
b	66.4	31.4	54.5	241	207	222	669	458	350	533	1,341	9.75	+0.79/−0.73	4.1	+0.27/−0.26	nm.	nm.	4.9
c	68.4	32.1	55.7	233	205	221	659	443	347	531	1,320	13.1	+0.99/−0.93	5.2	+0.31/−0.30	nm.	nm.	5.2
HPD#1333G05																		
a	75.0	26.0	ud.	201	184	198	583	ud.	ud.	ud.	ud.	210	+40/−30	330	+60/−45	nm.	71	—
b	70.1	19.4	ud.	157	138	147	443	ud.	ud.	ud.	ud.	191	+35/−27	400	+66/−51	nm.	74	—
c	72.2	17.5	ud.	139	124	133	396	ud.	ud.	ud.	ud.	170	+29/−22	400	+60/−48	nm.	nm.	—
d	73.0	36.2	ud.	285	256	275	817	ud.	ud.	ud.	ud.	163	+27/−21	200	+30/−24	nm.	77	—

HPD#1333G06																	
a	83.8	29.0	ud.	208	204	221	633	ud.	ud.	ud.	ud.	51.1	+6.8/−5.6	80	+12/−10	<20	nm.	—
b	89.4	33.3	ud.	228	233	253	714	ud.	ud.	ud.	ud.	51.3	+6.7/−5.5	70	+10/−9	<20	25	—
c	87.2	30.4	ud.	212	213	231	656	ud.	ud.	ud.	ud.	56.0	+7.2/5.9	80	+12/−10	<20	nm.	—
d	81.0	26.9	ud.	197	189	204	590	ud.	ud.	ud.	ud.	89.5	+16/−12	150	+30/−23	80	23	—
e	82.5	27.4	ud.	198	193	208	599	ud.	ud.	ud.	ud.	81.7	+13/−10	130	+25/−19	<20	nm.	—
f	82.9	28.5	ud.	206	200	217	623	ud.	ud.	ud.	ud.	76.6	+12/−9.2	120	+21/−17	<20	27	—
HPD#1333G07																		
a	63.9	31.0	0.621	241	202	216	658	5.27	3.94	5.99	15.2	88.7	+13/−10	50	+1.6/−1.6	nm.	nm.	nm.
b	67.5	30.4	0.702	230	200	214	644	5.81	4.49	6.86	17.2	106	+17/−14	52	+1.7/−1.6	nm.	nm.	nm.
c	68.8	24.1	0.557	180	158	170	507	4.54	3.55	5.43	13.5	121	+24/−18	56	+1.8/−1.7	nm.	nm.	nm.
d	78.2	32.1	9.43	207	199	216	622	66.4	56.9	88.0	211	65.8	+8.9/−7.4	28	+1.2/−1.2	nm.	nm.	nm.
HPD#1333G08																		
a	70.1	32.2	2.64	239	212	228	680	21.4	17.0	25.9	64.3	81.8	+11/−9.6	39	+1.4/−1.4	nm.	nm.	nm.
b	66.1	29.6	4.03	229	196	210	635	34.1	26.0	39.6	99.6	78.6	+11/−9.4	35	+1.4/−1.3	nm.	nm.	nm.
c	59.1	27.1	12.5	213	170	182	565	107	76.6	116	300	79.1	+11/−9.9	27	+1.2/−1.2	nm.	nm.	5.8
HPD#1333G11	67.5	33.6	42.7	218	193	210	620	303	239	369	911	20.3	+1.7/−1.6	9.0	+0.51/−0.49	nm.	nm.	nm.

ud. : under detection limit
— : radioactive equilibria
nm. : not measured

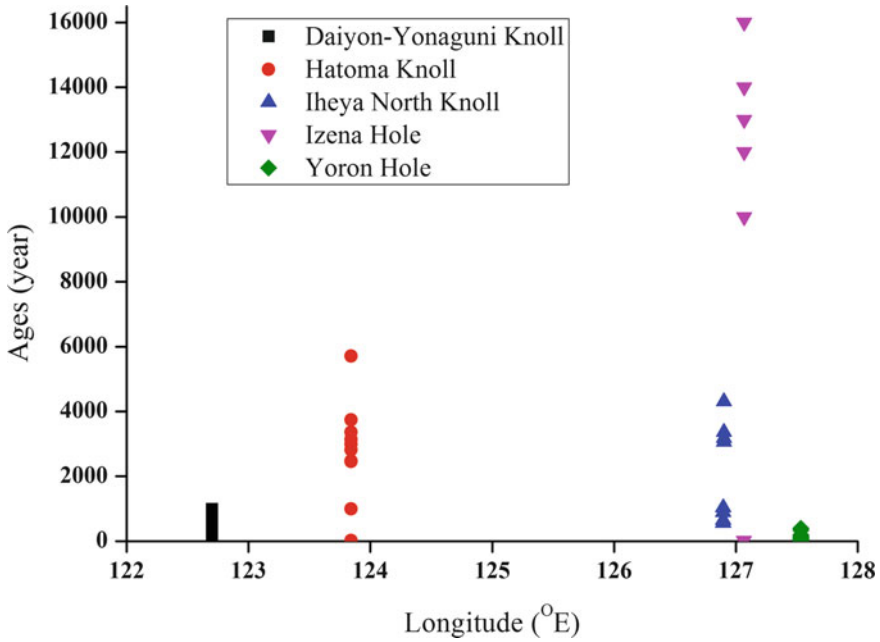

Fig. 29.6 The obtained ESR ages plotted as a function of longitude of the hydrothermal fields

References

Guérin G, Mercier N, Adamiec G (2011) Dose-rate conversion factors: update. Ancient TL 29:5–8

Hannington MD, Jonasson IR, Herzig PM, Petersen S (1995) Physical and chemical processes of seafloor mineralization at mid-ocean ridges. In: Humphris SE et al (eds) Seafloor hydrothermal systems; physical, chemical, biological, and geological interactions. American Geophysical Union Geophysical Monograph, vol 91, pp 115–157

Kasuya M, Kato M, Ikeya M (1991) ESR signals of natural barite ($BaSO_4$) crystals: possible application to geochronology. In Essay in Geology, Prof. Nakagawa Commemorative Volume: 95–98

Krystec M (1980) ESR measurements from X-ray irradiated $BaSO_4$ single crystals. Phys Status Solidi A 57:171–178

Noguchi T, Shinjo R, Ito M, Takada J, Oomori T (2011) Barite geochemistry from hydrothermal chimneys of the Okinawa Trough: insight into chimney formation and fluid/sediment interaction. J Mineral Petrol Sci 106:26–35

Okumura T, Toyoda S, Sato F, Uchida A, Ishibashi J, Nakai S (2010) ESR dating of marine barites in chimneys deposited from hydrothermal vents. Geochronometria 37:57–61

Sato F, Toyoda S, Banerjee D, Ishibashi J (2011) Thermal stability of ESR signals in hydrothermal barites. Radiat Meas 46:866–870

Takamasa A, Nakai S, Sato F, Toyoda S, Banerjee D, Ishibashi J (2013) U-Th radioactive disequilibrium and ESR dating of a barite-containing sulfide crust from South Mariana Trough. Quat Geochronol 15:38–46

Tivey MK (2007) Generation of seafloor hydrothermal vent fluids and associated mineral deposits. Oceanography 20:50–65

Toyoda S, Sato F, Banerjee D, Ishibashi J (2011) Characteristics of the radiation induced ESR signals in barite. Adv ESR Appl 27:4–6

Toyoda S, Sato F, Nishido H, Kayama M, Ishibashi J (2012) The alpha effectiveness of the dating ESR signal in barite. Radiat Meas 47:900–902

Toyoda S, Fujiwara T, Uchida A, Ishibashi J, Nakai S, Takamasa A (2014) ESR dating of barite in sulfide deposits formed by the sea floor hydrothermal activities. Radiat Prot Dosimetry 159:203–211

Yonezawa N, H. Matsue, Y. Miyamoto, D. Suzuki, K. Yasuda, J. Inagawa, Y. Saito (2002) Handbook for practical gamma ray spectrometry (Japanese title translated), Nikkan Kogyo, Japan. (Translation of Gilmore and Hemingway, 1995, Practical gamma-ray spectrometry, Wiley, Chichester/New York/Brisbane/Toronto/Singapore)

You CF, Bickle MJ (1998) Evolution of an active sea-floor massive sulphide deposit. Nature 394:668–671